 https://doi.org/10.3311/PPci.30373

Periodica Polytechnica Civil Engineering, 70(1), pp. 156–164, 2026

Algorithm for Generating Gradient Infills in Load-bearing 3D-printed Parts

David Juracka[1*], Martin Krejsa[1], Jiri Brozovsky[1]

[1] Department of Structural Mechanics, Faculty of Civil Engineering, VSB – Technical University of Ostrava, Ludvíka Podéště 1875/17, 708 00 Ostrava-Poruba, Czech Republic
[*] Corresponding author, e-mail: david.juracka@vsb.cz

Received: 15 January 2024, Accepted: 10 January 2026, Published online: 12 February 2026

Abstract

In many applications, it is crucial to design load-bearing elements that meet strength and stiffness requirements while minimizing material usage. Using additive manufacturing (AM), these goals can be achieved. With 3D printing technology is possible to create an internal structure — referred to as infill or lattice structure — generated by a dedicated algorithm. A special place is occupied by functionally graded lattice structures (FGLS), which are generated with tunable properties. which is the focus of this article. The primary objective of this algorithm is to create an internal parametric structure with variable thickness for any given cross-sectional shape. Secondary, the algorithm can calculate its cross-sectional characteristics. To evaluate its functionality and effectives, a series of 9 virtual models of cross-sections with 2 varying parameters were generated and subsequently compared with numerical models.

Keywords

3D printing, infill, algorithm, Rhino-Grasshopper, ANSYS

1 Introduction

Nowadays, science is rapidly pushing the boundaries of possibilities thanks to the development of robotics and machine learning. This area also includes additive manufacturing, which also includes 3D printing.

3D printing capabilities have grown tremendously in the last decade, and its influence can be found in almost every industry. The ability to produce an object based on a created or generated model has found practical application in every industry [1], e.g. design [2], construction [3], engineering, space [4], medicine [5, 6], and fashion [7]. At the same time, it is possible to work with different types of materials (plastic, metal, ceramics, tissue). There are many types of printers, but most of them are trying to achieve the highest efficient printing with different emphasis either on speed, strength, price, and weight.

A possible application in civil engineering is, for example, the creation of formwork for concrete structures that would otherwise be extremely difficult to manufacture [8]. A steel footbridge in Amsterdam was even built using a similar principle of technology [9], which works with shape optimization and organic design. Another use and potential benefit of 3D printing plastics is as reinforcement for concrete elements [10].

A separate and relatively widespread industry is 3D concrete printing (3DCP), which uses a similar principle to FFF/FDM technology (filament deposition modeling), but carries with it different challenges and tasks [11]. This area is not covered in the present article.

Every 3D-printed object consists of two parts, namely the outer cover (perimeter) and the infill. This inner structure is represented by a geometric pattern with open spaces. Thus, creates strong and lightweight support structure for a printed object. Currently, there are many geometric patterns (Fig. 1), which excel either in good-looking design, strength, or speed of 3D printing. Various articles were dedicated to investigate their effect on the resulting strength characteristics [12–17].

To optimize 3D printed elements with the aim of having a stronger and lighter element, two approaches can be used.

One works with the object's infill itself by changing its density. It is rather an intuitive procedure. For example, it is possible to increase the density only in some parts of the object or make it gradually towards the most stressed areas. This method is called gradient infill (see Fig. 2) [18], although it is not a smooth change of the infill density, which is created in individual sections, and it is a relatively lengthy manual process.

Cite this article as: Juracka, D., Krejsa, M., Brozovsky, J. "Algorithm for Generating Gradient Infills in Load-bearing 3D-printed Parts", Periodica Polytechnica Civil Engineering, 70(1), pp. 156–164, 2026. https://doi.org/10.3311/PPci.30373

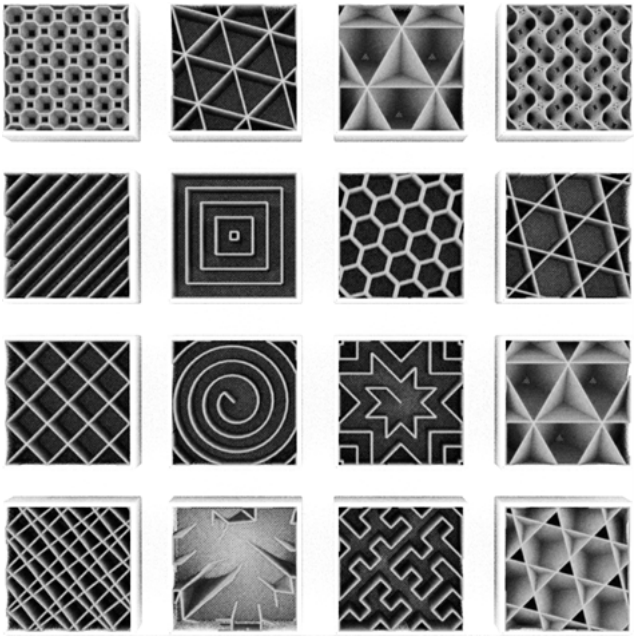

Fig. 1 Several examples of infill patterns in cross-section of 3D printed object

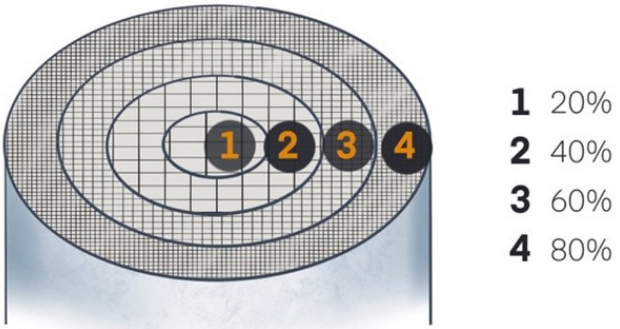

Fig. 2 Illustration of a cross-section with various density of infill

Another approach is to influence the extrusion of the material during printing. On the standard infill, the information about the material flow rate is changed in the generated gcode file containing instructions for the 3D printer. This is done using an algorithm [19, 20]. The result is a local reinforcement of the infill, which is created gradually, i.e. in a gradient infill (see Fig. 3). It is limited by the capabilities of the printing machine and the nozzle used. In this case, however, it is impossible to have a 3D object generated for evaluation by a numerical model.

The second approach uses computational software working with a numerical model, where supports and loads (its direction, type and magnitude) are defined. The result of such a model is a simulation with the plotting of areas of maximum stress curves. These areas are separated and a spatial model is subsequently created from them. This creates an optimized shape that can be produced using 3D printing [21, 22].

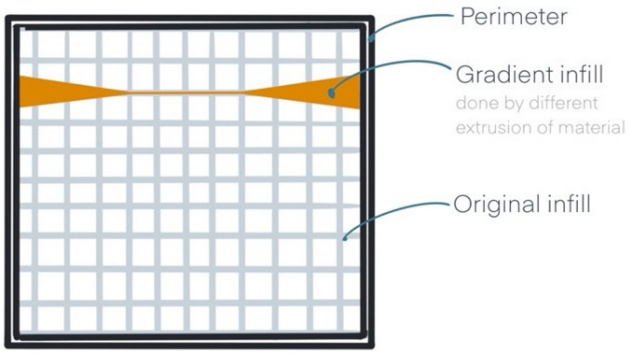

Fig. 3 Schematic representation of a cross-section with applied extrusion modification of infill

A special place is occupied by functionally graded lattice structures (FGLS), which work with the filling as an internal structure that can change its parameters such as size, pattern, thickness and many other parameters that can change smoothly from one area of the defined domain of the object to another. In simple terms, their basic principle is to generate a structure in a given domain (the overall shape of the object) based on a repeating part of the pattern, whether in 3D space or in a plane. Many software tools and procedures are available today to create FGLS, as well as a list of possible approaches to generating the resulting structure with the possibility of parameterization [23,24].

The internal structures created in this way gain additional variable properties in 3D printing. Because they form a separate 3D object, albeit inside the main 3D object, they again create the standard composition of perimeter and infill (see Fig. 4).

This article describes a custom designed algorithm that generates a planar cross-section with an internal gradient structure in any given shape. Subsequently, the algorithm calculates its cross-sectional characteristics.

This is a case study of working with the algorithm, a description of its creation, and a demonstration of a series of generated samples compared with a numerical model.

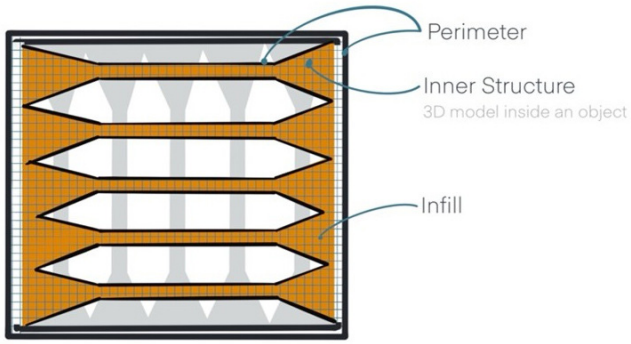

Fig. 4 Schematic representation of the gradient structure as an object with its infill

2 Methodology

The specific steps for creating the algorithm and its assessment were as follows:

- Create a parametric algorithm for generating a 2D internal structure;
- Create an algorithm for calculating the cross-sectional characteristics of the generated model;
- Generate a set of 9 cross-sections with two variable parameters for which the ratio between the area (i.e. the amount of material) and the elastic modulus will be calculated;
- Generate numerical models subjected to bending stress with a plot of von Mises stress;
- Overall evaluation of the effectiveness of the algorithm.

The parametric Rhino software [25] with the Grasshopper add-on was used to create the algorithm and a virtual model for further use in structural analysis software ANSYS [26].

The main principles of the procedure for creating a gradient structure in the final 2D cross-section are described in the following diagram (Fig. 5). The procedure can be summarized as follows:

1. Shape definition or import;
2. Definition of border thicknesses (including the radius of curvature around possible corners) and creation of rectangular grid of axes. The grid dimensions and rotation angle must be set;
3. The setting of distance gradient parameters is defined as a distance from the border to the point where the constant (minimal) starts. That is, the gradient is defined as a linear function. These parameters are set independently for both directions of the grid;
4. The setting of minimum thickness Then the basic (minimal) thickness of the internal structure and the maximum thickness are determined. The maximum thickness is set as a percentage of volume density, which depends on the distance between the axes;
5. The actual computation to create the gradient structure is created along the axes with the use of the abovementioned parameters;
6. A merge of all surfaces to create a single cross-sectional surface is created. It is also possible to round sharp corners in the internal structure.

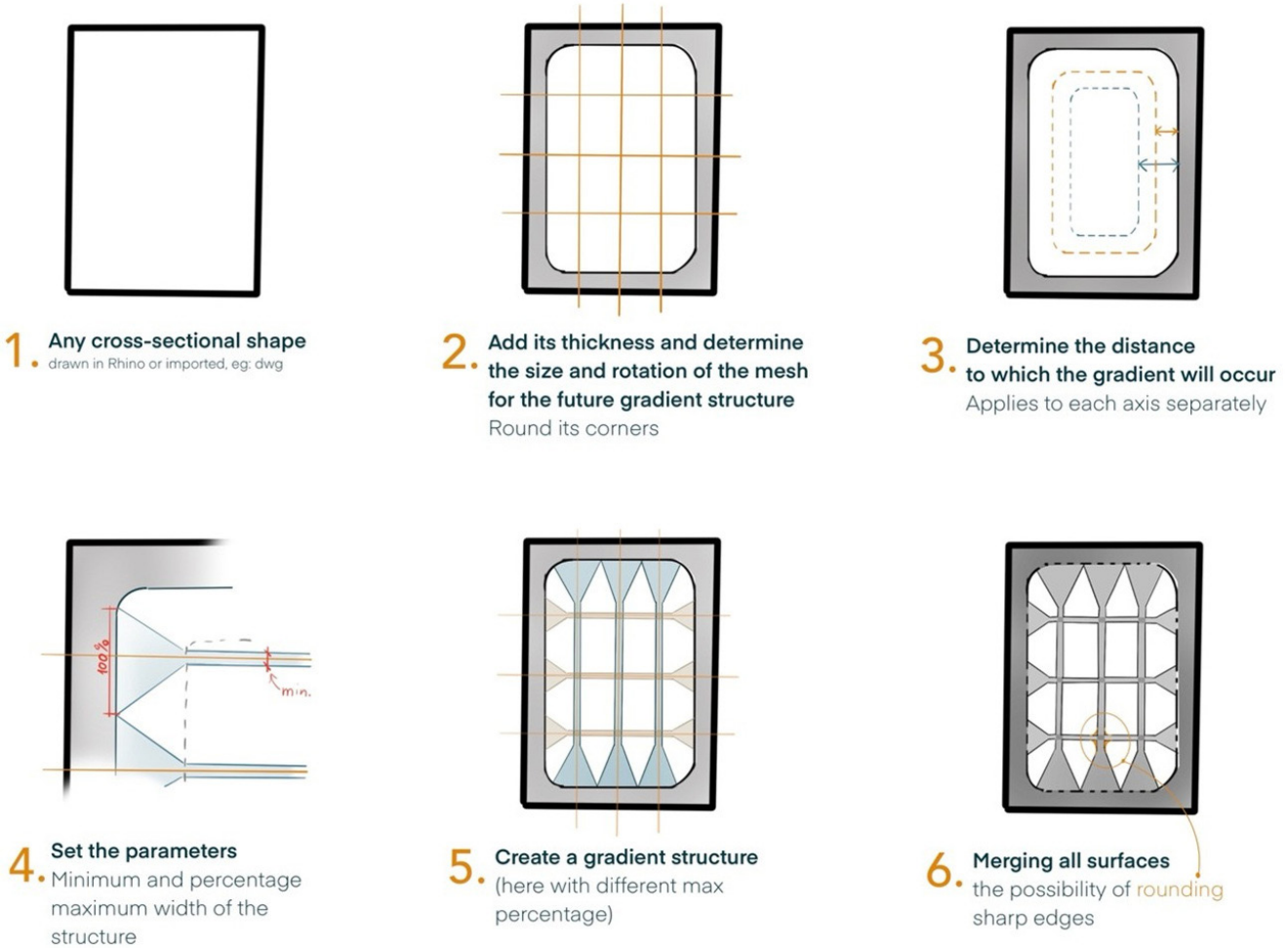

Fig. 5 Schematic representation of the basic principle of creating gradient structures

The implementation of the algorithm uses CAD functions of the Rhino software which are controlled by the user-defined program in Grasshopper (Fig. 6).

One of the advantages of the algorithm is that it can work with any cross-sectional shape, even imported from another program. Added functions allow for further modifications (see Fig. 6):

- If an axis of the grid enters the gradient formation zone, the thickness of the resulting structure changes depending on the distance from the boundary of this zone;
- It is possible to add a point or curve modifier to locally increase the thickness of the structure. It works on the same principle as the already described function (with its setting of the domain of influence and target thickness).
- It is also possible to deal with pre-defined (imported) openings or holes. Around these openings, it is possible to define the change in thickness of the structure and the thickness of the wall around the opening.
- The last feature is the ability to change the linear function depending on the distance from the edge of the inner wall for creating gradient thickness of the structure. This is achieved by adding curve directions at regional points. This softens the sharp transitions in the shapes.

These are all functions of the algorithm that can be combined in such a way that their influence adds up but does not exceed a maximum limit, for example, exceeding the maximum possible thickness.

A second part of the algorithm can be used to calculate cross-sectional characteristics, which works independently and can also be used for separately imported cross-sections. It works with any shape and added holes. It calculates area and determine the center of gravity, moment of inertia, deviating moment, section modulus, a radius of inertia, and polar moment. These results are automatically saved to a .txt file on your desktop. It is also possible to generate a beam by pulling out the cross-section, which can be exported as a 3D object in various formats (see Fig. 7).

The principle of calculating the characteristics lies in the fitting of more easily definable squares (with a clear area and center of gravity). However, a problem arises when the edges of these squares do not completely merge with the shape of the cross-section, resulting in calculation inaccuracy. This accuracy can be greatly approved by reducing the dimension of these squares, although at the expense of computing power.

The overall program diagram of both algorithms is shown in Scheme 1.

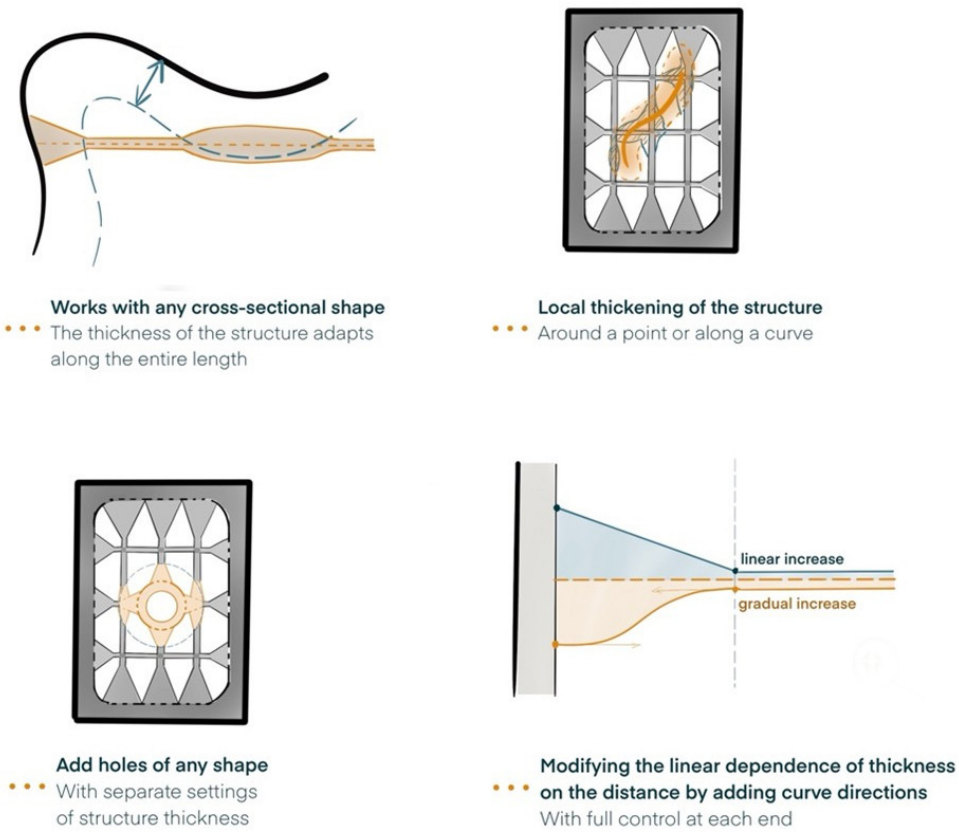

Fig. 6 Schematic representation of additional functions of the gradient structure algorithm

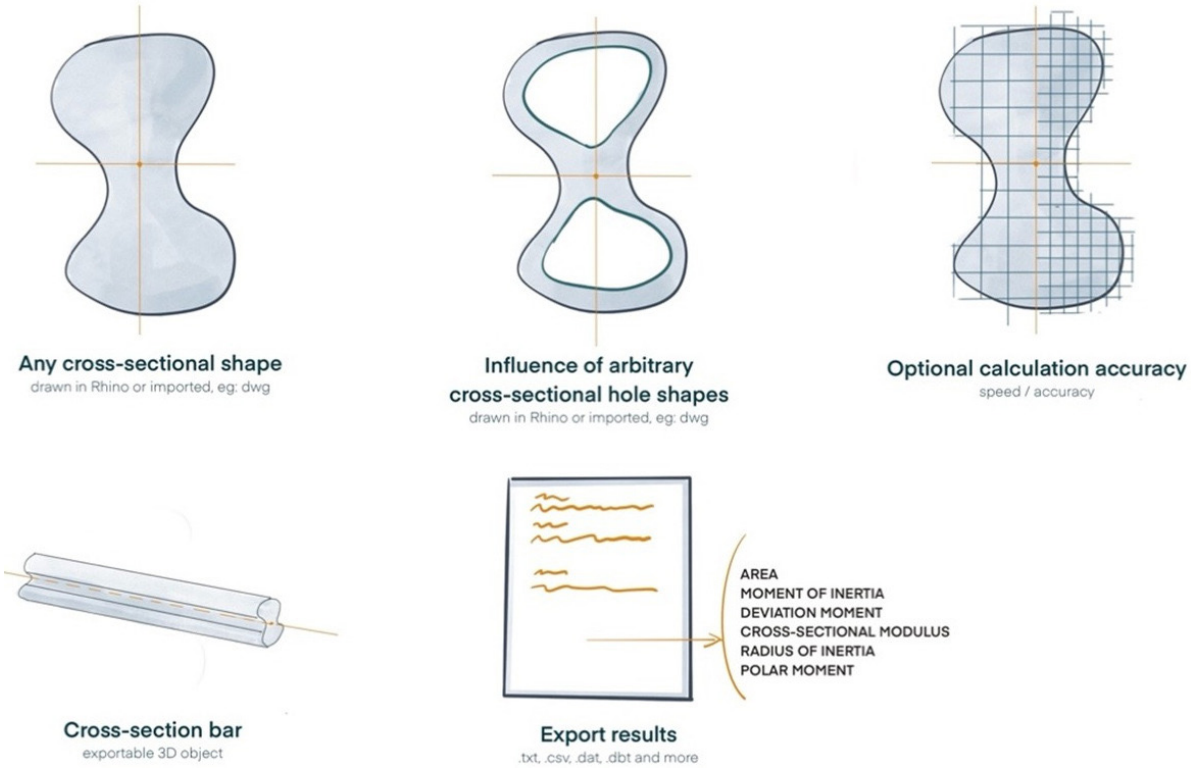

Fig. 7 The main features of the algorithm for calculating cross-section characteristics

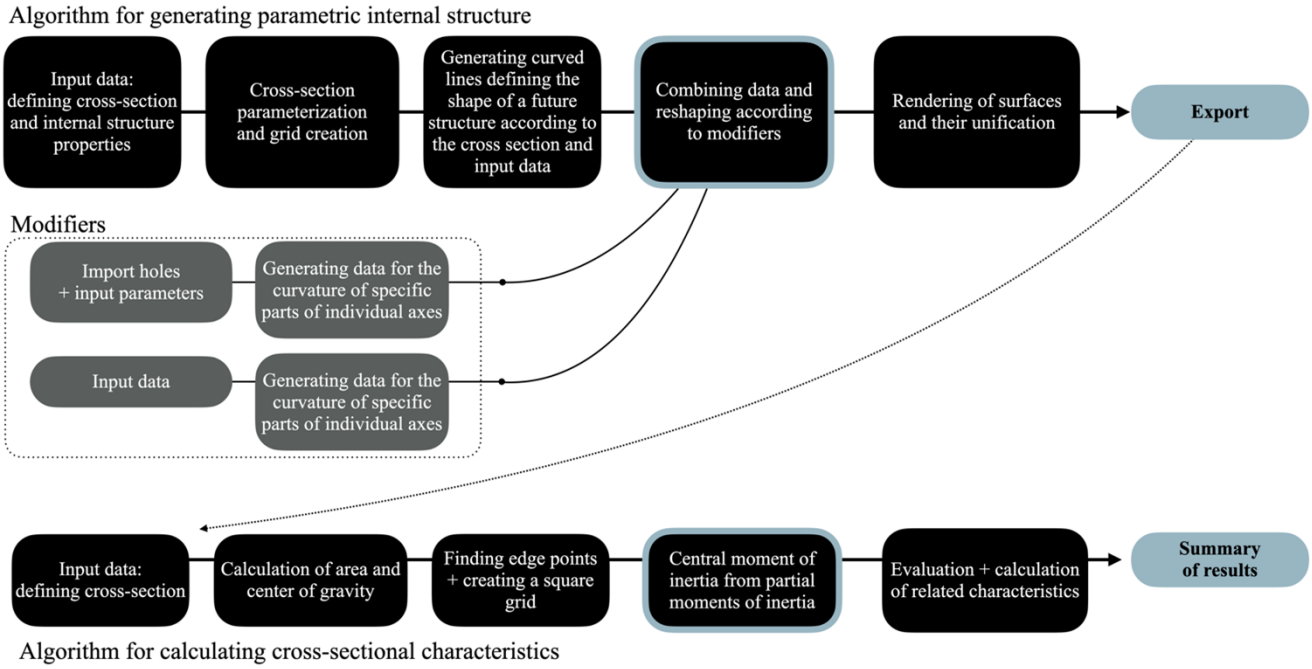

Scheme 1 The overall program diagram of both algorithms

3 Generating a series of cross-sections and their numerical analysis

With the algorithm a series of 9 cross-sections were generated for numerical analysis. To make it simple, a rectangular shape was chosen with dimensions 20 × 40 mm. There are many combinations of possible factors to choose from, therefore, the 2 most affecting ones were selected (see Fig. 8):

- The extension factor of domain for change of structure thickness given by the ratio of distances between the direction of the y-axis (which does not change further) to the z-axis. In three values: 1.0×, 1.5×, 2.0×

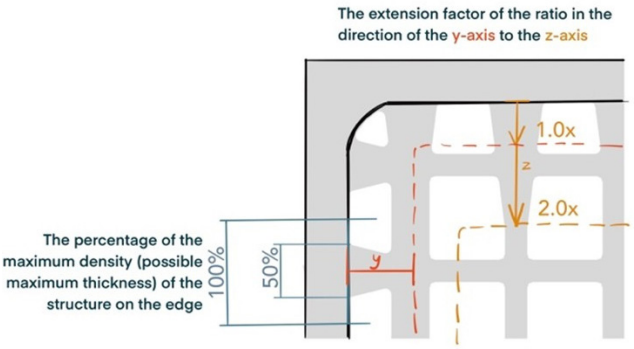

Fig. 8 The scheme of changing factors for generating the resulting internal structure

- The percentage of the maximum density (possible maximum thickness) of the structure on the edge of the cross-section wall, which is the same for both axes. In three values: 50%, 75%, 100%.

Resulting series of generated cross-sections with internal structure is depicted in Fig. 9 including values of area size and cross-sectional modulus relative to the *y*-axis. These generated cross-sections form a beam with a length of 220 mm, which was loaded according to Scheme 2 for four-point bending. The loading was carried out within the framework of the simulation of the numerical model in the ANSYS software [26]. This beam was loaded so that the upper supports were shifted 1 mm down, thus introducing stress into the beam. The material properties were selected according to the PC Blend filament used for 3D printing with FFF/FDM technology, while for the purposes of the article, the mechanical properties of the material such as the direction of the printed fibers were not included. The material is homogeneous and isotropic with the following selected properties: Young's modulus 1 900 MPa; tensile yield strength 63 MPa; density 1.22e-09 t/mm^3. A total of nine numerical models are created, in which the resulting stress is evaluated after loading and compared with the cross-sectional characteristics.

4 Evaluation of numerical models

All models were evaluated for equivalent stress according to von Mises (see Fig. 10). The figure shows a cross-section of each model at the location of the internal support, which generates local stresses in the cross-section that propagate further along the internal structure. Therefore, these stresses are greater in the upper part of the cross-section. This location was deliberately chosen because of the more pronounced influence of the stress profile around the internal holes. For comparison, the stress values were given at several places along the height of the cross-section, where the transverse structures generated by the algorithm also intersect.

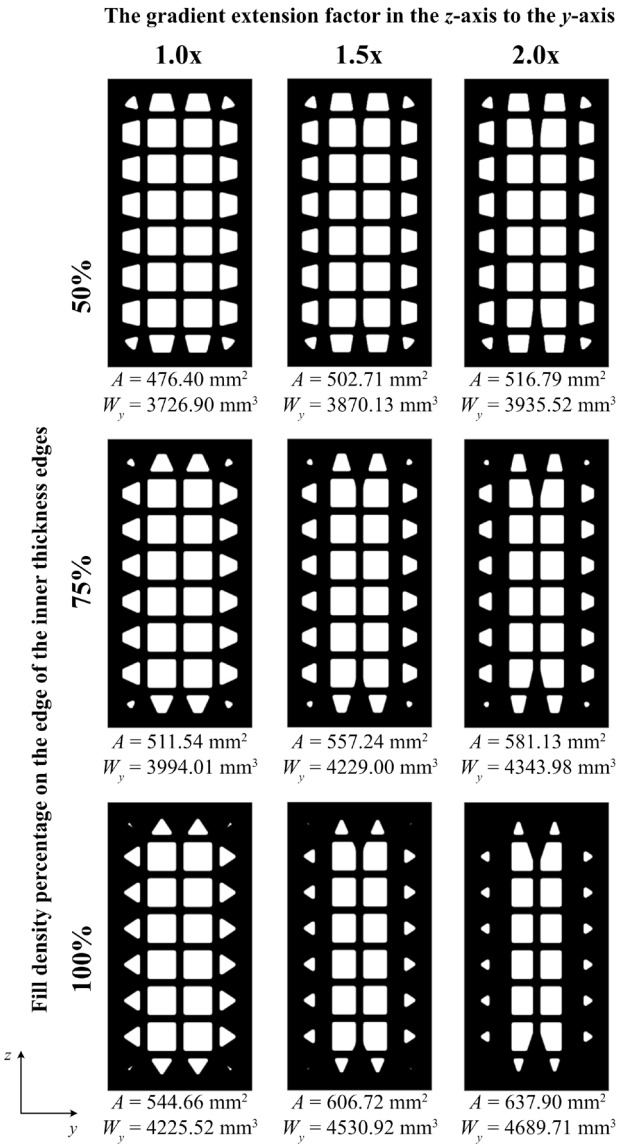

Fig. 9 The scheme of generated cross-sections with internal structure

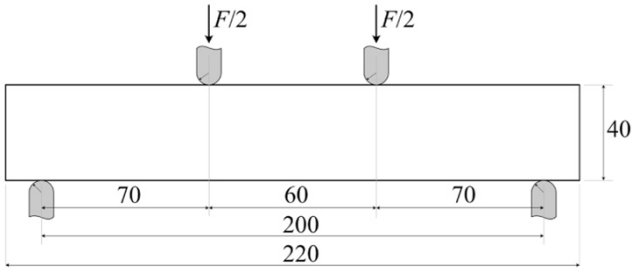

Scheme 2 Side view of a beam loaded with four-point bending

When comparing individual cross-sections, the influence of density (50%, 75%, and 100%) on the resulting stress values can be evaluated first. For the uppermost evaluated point, an inverse relationship between pattern density and stress is observed: increasing density leads to lower stress values. This effect becomes even more pronounced when combined with a higher gradient elongation factor. Based on

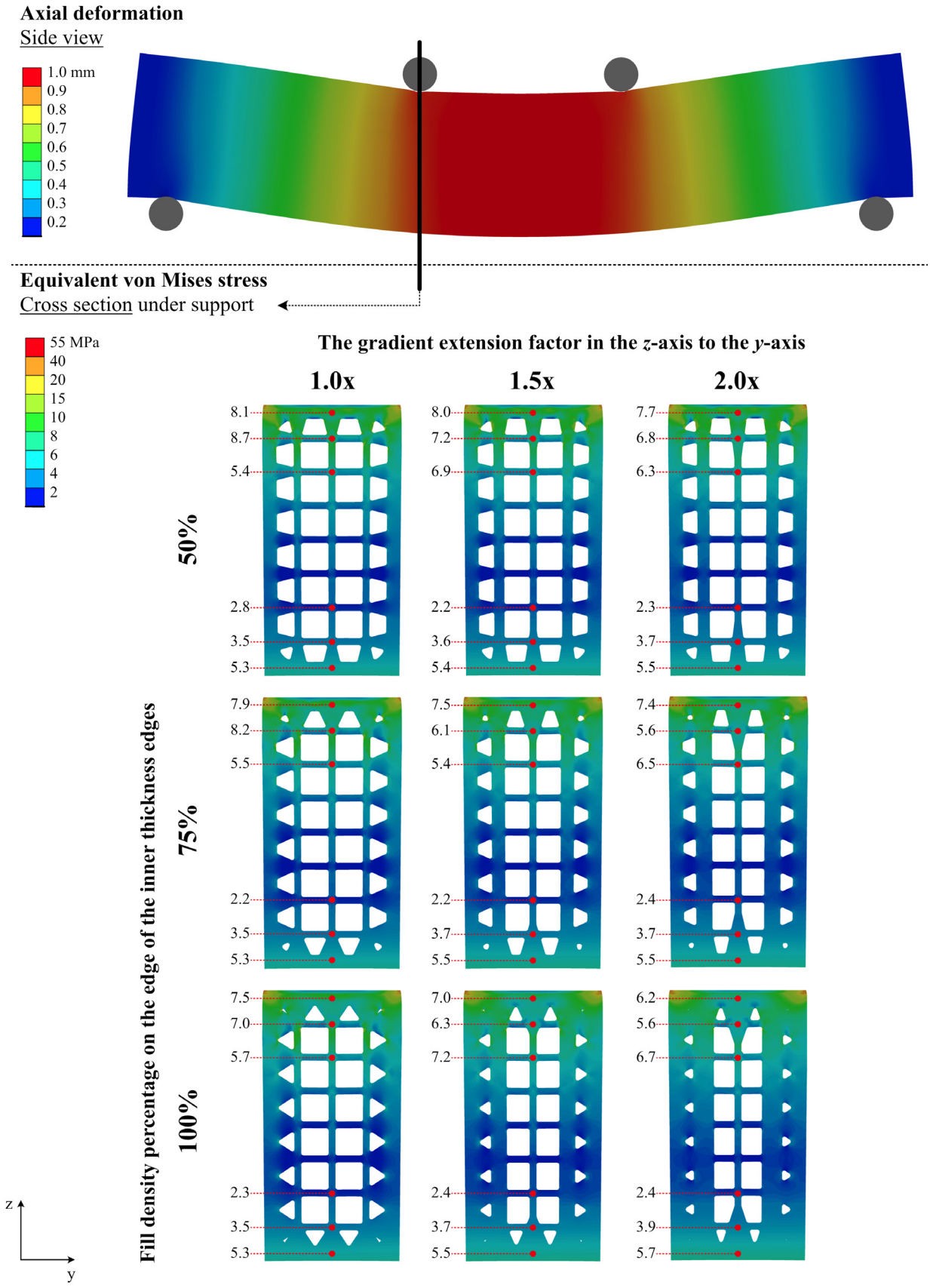

Fig. 10 Results in the representation of the von Mises equivalent stress

these results, it can be clearly stated that the cross-section with 50% density and a gradient elongation factor of 1.0 exhibited the highest stress value (8.1 MPa), whereas the cross-section with 100% density and a factor of 2.0 showed the lowest stress value (6.2 MPa).

All stress values measured at the top side of the cross-sections are summarized in Table 1, together with the corresponding cross-sectional area (A) and section modulus (W_y). It follows that the first sample, despite exhibiting the highest stress, has the smallest area and therefore the lowest material consumption, but also the smallest section modulus. In contrast, the second sample shows the opposite trend, combining a larger area and section modulus with reduced stress levels.

A similar trend can also be observed for the remaining stress values along the height of the cross-section, with slightly higher stresses consistently occurring at the narrowest part of the gradient transition. However, the magnitude of this stress decreased with increasing gradient elongation factor. This behavior can be explained by the greater distance from the upper edge of the entire cross-section, where the stress values reach their maximum.

In summary, the gradient change in thickness primarily influenced the stress distribution through the size of the area over which the stress was dispersed–especially in the widest part of the cross-section–and the extent of this distribution along the height.

The stress results in the lower part of the cross-section exhibit a different trend, which can largely be attributed to the fact that the section was evaluated beneath the loading support.

At this stage, the generated cross-sections are not optimized and should be understood as a demonstration of the application of the developed algorithm. The reported stress values and the efficiency in terms of material savings (i.e., achieving a smaller cross-sectional area) were strongly influenced by the increase in thickness of the internal structure along the height of the cross-section, particularly in regions closer to the edges. As a result, these regions entered the domain of the gradient thickness variation and, due to their parallel orientation to the side walls, retained a constant thickness. Nevertheless, these effects can be adjusted as needed depending on the loading conditions and design requirements.

Table 1 Comparison of the resulting numerical values of samples with a gradient structure.
The best (green) and worst (orange) result in each section is always highlighted.

Density (%)	Extension factor	A (mm^2)	W_y (mm^3)	σ (MPa)
	1.0 x	**476.40**	**3726.90**	**8.1**
50	1.5 x	502.71	3870.71	8.0
	2.0 x	516.79	3935.52	**7.7**
	1.0 x	511.54	3994.01	7.9
75	1.5 x	557.24	4229.00	7.5
	2.0 x	581.13	4343.98	7.4
	1.0 x	544.66	4225.52	**7.5**
100	1.5 x	606.72	4530.92	7.0
	2.0 x	**637.90**	**4689.71**	**6.2**

5 Conclusions

An algorithm was created to construct a gradient structure within a defined external cross-sectional shape.

With the structure created in this way, it was then possible to calculate the cross-sectional characteristics via the second algorithm created.

To assess the effectiveness of work with the cross-section, a series of 9 samples was created focusing on 2 factors - the percentage density (from the possible thickness) of the material at the inner edge of the cross-section and the coefficient of the factor of the extension of the domain for formation of linear thickening structure in the z-axis compared to the y-axis.

The aim of the article and the algorithm created was to explore another way of creating an internal parametric structure with variable thickness - its functionality and impact on the effective distribution of mass in the cross-section with an impact on the cross-sectional modulus and the occurrence of stress concentration sites. Although this is certainly not a clear shift in science, it is another way of working with topological optimization. The use of topology has applications, for example, in 3D printing in various fields, including construction.

In the production of such samples, the possibilities of additive manufacturing, namely 3D printing, would be used. For example, it would be possible to use the most common FFF/FDM technology in combination with a stronger material such as PC (polycarbonate). This technology is characterized by printing fibers in layers, where the overall strength of the sample depends on the direction of these fibers, which can be influenced.

Acknowledgment

The financial support of the grant program financed by the Ministry of Education, Youth and Sports of the Czech Republic through VSB – TU Ostrava SGS SP2022/96.

References

[1] Shahzad, Q., Umair, M.,Waqar, S. "Bibliographic analysis on 3D printing in the building and construction industry: Printing systems, material properties, challenges, and future trends", Journal of Sustainable Construction Materials and Technologies, 7(3), pp. 198–220, 2022. https://doi.org/10.47481/jscmt.1143239

[2] Ivanov-Kostetskyi, S., Gumennyk, I.,Voronkova, I. "Innovative Trends in Architecture – Creating Full-Scape Buildings with the 3D Print Technology", IOP Conference Series: Materials Science and Engineering, 1203(2), 022099, 2021. https://doi.org/10.1088/1757-899X/1203/2/022099

[3] Qi, L., Bai, J., Huang, Q., Yang, Y., Han, L., Yue, C., Yan, Z. X. "Mobile 3D Printing Techniques for Construction Engineering: Outdoor Navigation and Printing Quality Control", Structural Engineering International 32(2), pp. 203–210, 2022. https://doi.org/10.1080/10168664.2022.2025749

[4] National Research Council "3D Printing in Space", Academies Press, 2014. ISBN 978-0-309-31008-6 https://doi.org/10.17226/18871

[5] Peleshok, S. A., Golovko, K. P. "3D printing and medicine", Russian Military Medical Academy Reports, 41(3), pp. 325–333, 2022. https://doi.org/10.17816/rmmar88645

[6] Sandhu, K., Singh, S., Prakash, C., Subburaj, K., Ramakrishna, S. "3D Printing in Podiatric Medicine". Academic Press, 2023. ISBN 978-0-323-91911-1. https://doi.org/10.1016/C2021-0-00378-3

[7] Kam, S. "Three-Dimensional Printing Fashion Product Design with Emotional Durability Based on Korean Aesthetics" Sustainability, 14(1), 240, 2022. https://doi.org/10.3390/su14010240

[8] Jipa, A., Dillenburger, B. "3D Printed Formwork for Concrete: State-of-the-Art, Opportunities, Challenges, and Applications", 3D Printing and Additive Manufacturing, 9(2), pp. 84–107, 2022. https://doi.org/10.1089/3dp.2021.0024

[9] MX3D "MX3D Bridge", [online] Available at: https://mx3d.com/industries/mx3d-bridge/ [Accessed: 26 February 2025]

[10] Katzer, J., Szatkiewicz, T. "Effect of 3D Printed Spatial Reinforcement on Flexural Characteristics of Conventional Mortar", Materials, 13(14), 3133, 2020. https://doi.org/10.3390/ma13143133

[11] Federowicz, K., Techman, M., Skibicki, S., Chougan, M., El-Khayatt, A. M., Saudi, H. A., Błyszko, J., Abd Elrahman, M., Chung, S. Y., Sikora, P. "Development of 3D printed heavyweight concrete (3DPHWC) containing magnetite aggregate", Materials & Design, 233, 112246, 2023. https://doi.org/10.1016/j.matdes.2023.112246

[12] Mishra, P. K., Senthil, P., Adarsh, S., Anoop, M. S. "An investigation to study the combined effect of different infill pattern and infill density on the impact strength of 3D printed polylactic acid parts", Composites Communications, 24, 100605, 2021. https://doi.org/10.1016/j.coco.2020.100605

[13] Chacón, J. M., Caminero, M. A., García-Plaza, E., Núñez, P. J. "Additive manufacturing of PLA structures using fused deposition modelling: Effect of process parameters on mechanical properties and their optimal selection", Materials & Design, 124, pp. 143–157, 2017. https://doi.org/10.1016/j.matdes.2017.03.065

[14] Dudescu, C., Racz, L. "Effects of Raster Orientation, Infill Rate and Infill Pattern on the Mechanical Properties of 3D Printed Materials", ACTA Universitatis Cibiniensis, 69(1), pp. 23–30, 2017. https://doi.org/10.1515/aucts-2017-0004

[15] Juracka, D., Kawulok, M., Bujdos, D., Krejsa, M. "Influence of Size and Orientation of 3D Printed Fiber on Mechanical Properties under Bending Stress", Periodica Polytechnica Civil Engineering, 66(4), pp. 1071–1076, 2022. https://doi.org/10.3311/PPci.19806

[16] Alejandrino, J. D., Ronnie S., Lauguico, S. C., Tobias, R. R.,Venancio, L., Macasaet, D., Bandala, A. A., Dadios, E. P. "A Machine Learning Approach of Lattice Infill Pattern for Increasing Material Efficiency in Additive Manufacturing Processes", International Journal of Mechanical Engineering and Robotics Research, 9(9), pp. 1253–1263, 2020. https://doi.org/10.18178/ijmerr.9.9.1253-1263

[17] Protolabs Network "Selecting the optimal shell and infill parameters for FDM 3D printing", [online] Available at: www.hubs.com/knowledge-base/selecting-optimal-shell-and-infill-parameters-fdm-3d-printing/ [Accessed: 19 June 2022]

[18] Maszybrocka, J., Dworak, M., Nowakowska, G., Osak, P., Łosiewicz, B. "The Influence of the Gradient Infill of PLA Samples Produced with the FDM Technique on Their Mechanical Properties", Materials, 15(4), 1304, 2022. https://doi.org/10.3390/ma15041304

[19] CNC Kitchen "Gradient infill for 3D prints", [online] Available at: https://www.cnckitchen.com/blog/gradient-infill-for-3d-prints [Accessed: 19 June 2022]

[20] "Dynamic Infill Density in the new KISSlicer v2 alpha", [online] 2019. https://www.sublimelayers.com/2019/05/dynamic-infill-density-in-new-kisslicer.html

[21] Gil, B., Goñi, R., Fábregas, M., Bayo, E. "Proposal and experimental verification of additive manufactured beam-column connection designed by topological optimization", Ce/papers, 6(3–4), pp. 702–707, 2023. https://doi.org/10.1002/cepa.2490

[22] Xin, Q. C., Yang, L., Huang, Y. N. "Digital design and manufacturing of spherical joint base on multi-objective topology optimization and 3D printing", Structures, 49, pp. 479–491, 2023. https://doi.org/10.1016/j.istruc.2023.01.101

[23] Veloso, F., Gomes-Fonseca, J., Morais, P., Correia-Pinto, J., Pinho, A. C. M., Vilca, J. L. "Overview of Methods and Software for the Design of Functionally Graded Lattice Structures", Advanced Engineering Materials, 24(11), 2200483, 2022. https://doi.org/10.1002/adem.202200483

[24] Stragiotti, E. "Continuous Fiber Path Planning Algorithm for 3D Printed Optimal Mechanical Properties", MSc Thesis, Politecnico di Torino, 2020. https://doi.org/10.13140/RG.2.2.30196.07046

[25] Robert McNeel & Associates "Rhinoceros, (v8)", [computer program] Available at: https://www.rhino3d.com/8/new/ [Accessed: 12 January 2023]

[26] ANSYS "Engineering Simulation Software, (2024 R2)", [computer program] Available at: https://www.ansys.com/webinars/ansys-2024-r2-discovery-whats-new [Accessed: 10 January 2023]